

1 **Estimating the sensitivity of the Priestley-Taylor coefficient to air**
2 **temperature and humidity**

3 Ziwei Liu, Hanbo Yang *, Changming Li, Taihua Wang

4 State Key Laboratory of Hydro-science and Engineering, Department of Hydraulic
5 Engineering, Tsinghua University, Beijing, China

6 *Correspondence to:* Hanbo Yang (yanghanbo@t2singhua.edu.cn)

7 Abstract

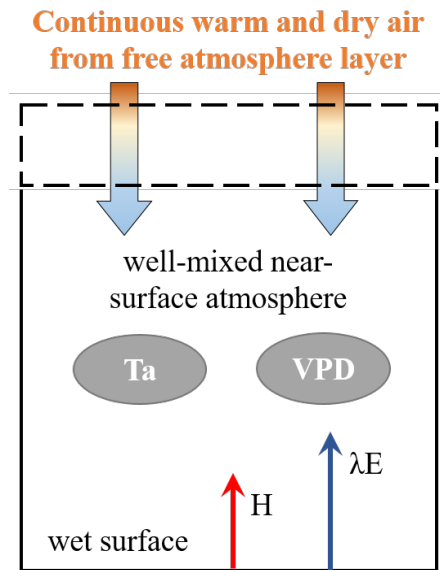
8 Priestley-Taylor (PT) coefficient (α) is generally set as a constant value or fitted as an
9 empirical function of environmental variables, and it can bias the evaporation estimation
10 or hydrological projections under global warming. By using an atmospheric boundary
11 layer model, this study derives a theoretical and parameter-free equation for estimating α
12 as a function of air temperature (T) and specific humidity (Q). With observations from
13 several water bodies and non-water-limited land sites, we demonstrate that in addition to
14 well estimating the value of α , the derived expressions can also capture the sensitivity of
15 α to T and Q, that is, $d\alpha/dT$ and $d\alpha/dQ$. α is generally negatively associated with T and Q,
16 of which T plays a more fundamental role in controlling α behaviors. Based on climate
17 model data, we further show that this negative relationship between α and T is of great
18 importance for long-term hydrological predictions. We also provide a lookup graph for
19 practical and broad uses to directly find the values of $d\alpha/dT$ and $d\alpha/dQ$ under specific
20 conditions. Overall, the derived expression gives a physically clear and straightforward
21 approach to quantify changes in α , which is essential for PT-based hydrological
22 simulation and projections.

23 1. Introduction

24 Evaporation from wet surfaces, including oceans, lakes, and reservoirs, is relevant to
 25 global hydrological cycles and water availability. There is a long history of developing
 26 theories and methods to estimate wet surface evaporation [Bowen, 1926; Penman, 1948;
 27 Priestley and Taylor, 1972; Thornthwaite and Holzman, 1939; Yang and Roderick, 2019].
 28 Among existing models, the Priestley-Taylor (PT) model/equation is known for its
 29 transparent structure and low input requirement [Priestley and Taylor, 1972]. The PT
 30 equation is widely used in evaporation estimation across varied scales and is the basis for
 31 various hydrologic and land surface models. Specifically, the PT equation comes from
 32 the equilibrium evaporation (λE_{eq}), and λE_{eq} can be calculated as [Slatyer and McIlroy,
 33 1961]:

$$34 \quad \lambda E_{eq} = \frac{\varepsilon_a}{\varepsilon_a + 1} (R_n - G) \quad (1)$$

35 where λ (J/kg) is the latent heat of water vaporization, $\varepsilon_a = \Delta/\gamma$, Δ (kPa/K) is the slope of
 36 the saturated vapor pressure versus temperature curve (a function of temperature), and γ
 37 is the psychrometric constant. ε_a is a function of air temperature (T). $R_n - G$ (kPa/K) is the
 38 available energy. The equilibrium evaporation indicates that the near-surface air is
 39 saturated, supposing the vapor pressure deficit (VPD) is zero. However, it does not exist
 40 in the real world [Brutsaert and Stricker, 1979; J.P. Lhomme, 1997a], due to the
 41 continuous exchanges of warm and dry air from the entrainment layer, although water is
 42 continuously transported from the bottom wet surface into the atmosphere through
 43 evaporation process (Figure 1).



44

45 Figure 1. Atmospheric boundary layer box model describing the energy and water fluxes
 46 at the saturated surface and atmosphere above. The dotted line represents the removable
 47 upper boundary of the box. H and λE are the sensible and latent heat fluxes. T_a is the air

48 temperature and VPD is the vapor pressure deficit.

49

50 In this case, the PT equation introduced a parameter, α , known as the PT coefficient, to
51 estimate wet surface evaporation [*Priestley and Taylor, 1972*]. α represents the effects of
52 vertical mixing of dry and moist air and adjusts the equilibrium evaporation to the actual
53 evaporation. So qualitatively speaking, the α is impossibly lower than one because the air
54 is always not saturated and can only infinitely close to saturated condition, no matter how
55 moist the near-surface air is. The PT equation is:

$$56 \quad \lambda E = \alpha \frac{\epsilon_a}{\epsilon_a + 1} (R_n - G) \quad (2)$$

57 In the original study of *Priestley and Taylor* [1972], the value of α is fitted as 1.26. While
58 a fixed α value can reasonably estimate wet surface evaporation [*Yang and Roderick,*
59 2019], some studies found that α varies across time and space, for example, α often shows
60 a more prominent value under cold conditions and becomes lower as warms [*Debruin*
61 *and Keijman, 1979; Xiao et al., 2020*]. This indicates that α should be a variable rather
62 than a constant [*Assouline et al., 2016; Crago et al., 2023; Eichinger et al., 1996; Guo et*
63 *al., 2015; Jury and Tanner, 1975; J. P. Lhomme, 1997b; Maes et al., 2019; McNaughton*
64 *and Spriggs, 1986; van Heerwaarden et al., 2009*]. However, the hydrology field
65 predominantly employs the fixed value of $\alpha = 1.26$, despite those earlier findings being
66 over three decades old.

67 A general method to quantify the changes in α is to inverse it with observations based on
68 Equation (2) and then build relationships among α and investigated variables. Since a
69 negative relationship between α and temperature (T) is a consensus from multi-scale
70 observations [*Assouline et al., 2016; Xiao et al., 2020*], many attempts empirically fitted
71 α as a function of T [*Andreas and Cash, 1996; Hicks and Hess, 1977; Yang and Roderick,*
72 2019]. Recent work further showed that the air humidity state can also influence the
73 spatiotemporal patterns of α [*Su and Singh, 2023*]. While those methods promote our
74 understanding of the potential variations in α , they more lie on the empirical side and pay
75 less attention to the underlying process. Hence, various endeavors have been made to
76 calculate α through physical means, but they are often constrained by the complexity of
77 numerous parameters. For instance, in the research conducted by *J. P. Lhomme* [1997b],
78 α was explicitly formulated utilizing the PM model in conjunction with boundary layer
79 theory. Nevertheless, the formulation incorporates parameters that signify surface and
80 aerodynamic resistances, making them hard to determine through direct measurements.
81 Subsequently, by using a refined boundary layer model, *van Heerwaarden et al.* [2009]
82 introduced a mathematical expression for estimating α , however, the expression also
83 involves a set of parameters necessitating numerical experiments to delineate a feasible
84 range for α . Consequently, obtaining a precise α estimation using conventional
85 observations still has remained a challenge.

86 Based on a recent study by *Z Liu and Yang* [2021], here we aim to derive a physically
 87 clear, transparent, and calibration-free equation for estimating α , by introducing a
 88 governing equation (potential vapor pressure deficit budget) into the conventional
 89 boundary layer model. In the following sections, we will first provide the theory for
 90 estimating α and its sensitivity to climate conditions: air temperature (T) and humidity
 91 (represented by the air specific humidity, Q). We further evaluate the theory based on
 92 measurements from the water and non-water-limited land surfaces, followed by the
 93 influences of α changes on long-term hydrologic projections.

94 2. Theory

95 2.1 Derivation of Bowen ratio

96 Here, we use an atmospheric boundary layer-based (ABL) model as the basis for the
 97 Bowen ratio (defined as the ratio of sensible heat fluxes to latent heat fluxes, $H/\lambda E$)
 98 derivation [*Z Liu and Yang*, 2021]. The fundamental conservation equations for states of
 99 moisture and energy over the water surfaces are [*Raupach*, 2001]:

$$100 \quad \rho c_p \frac{d\theta}{dt} = \frac{H}{h} + \frac{\rho c_p g_e}{h} (\theta_e - \theta) \quad (3)$$

$$101 \quad \rho \lambda \frac{dQ}{dt} = \frac{\lambda E}{h} + \frac{\rho \lambda g_e}{h} (Q_e - Q) \quad (4)$$

102 where θ (K) is the potential temperature, Q is the specific humidity, c_p (J/kg/K) is the
 103 specific heat capacity of air at constant pressure, g_e (m/s) is the entrainment flux velocity
 104 into the ABL box, and h (m) is the height of the ABL. The subscript e indicates the
 105 variable is evaluated at the upper boundary of the ABL (see Figure 1).

106 According to Equations (3) and (4), we can obtain a formula to calculate the rate of VPD
 107 ($dVPD/dt$, see details in *Z Liu and Yang* [2021]):

$$108 \quad \frac{dVPD}{dt} = \frac{\epsilon_a H - \lambda E}{\rho \lambda h} + \frac{g_e}{h} \Delta_D \quad (5)$$

109 where Δ_D is calculated as:

$$110 \quad \Delta_D = VPD_e - VPD \quad (6)$$

111 Under the state that air is saturated, the water vapor is continuously transported from the
 112 water surface to the atmosphere, keeping the air saturated. In this case, there is no vertical
 113 moisture gradient, that is, the air near the surface and the air at the upper boundary of the
 114 ABL should be saturated, so VPD and VPD_e are both equal to zero. With Equation (6),
 115 we can know $\Delta_D = 0$.

116 When air is not saturated, we can rewrite Equation (6) as:

$$117 \quad \Delta_D = Q - Q_e + [Q_{\text{sat}}(\theta_e) - Q_{\text{sat}}(\theta)] \quad (7)$$

118 where Q_e is much smaller than Q , and $Q_{\text{sat}}(\theta_e) - Q_{\text{sat}}(\theta)$ is small (one order of magnitude
119 smaller than Q), so the Δ_D roughly equals Q [Z Liu and Yang, 2021; Raupach, 2001].

120 Under a relatively long-term (monthly and/or longer), there is a potential VPD budget
121 ($d\text{VPD}/dt = 0$) over water surfaces [Raupach, 2001], and g_e can be estimated as the
122 function of H and λE as:

$$123 \quad g_e = \frac{H + \Lambda \cdot \lambda E}{\rho c_p \gamma_v h} \quad (8)$$

124 where Λ is a constant (0.07), and γ_v is the potential virtual temperature gradient in the
125 free atmosphere above the ABL. $\gamma_v h$ can be set as a fixed value of 7 K [Z Liu and Yang,
126 2021]. Combining with the VPD budget, Equation (5) and (8), we can obtain the
127 expression for Bo :

$$128 \quad \text{Bo} = \begin{cases} \frac{1}{\varepsilon_a}, \text{equilibrium} \\ \frac{1 - \Lambda \chi}{\varepsilon_a + \chi}, \text{non-equilibrium} \end{cases} \quad (9)$$

129 where $\chi = \frac{\lambda Q}{c_p \gamma_v h}$, a function of Q .

130 **2.2 Theoretical formula for α**

131 The surface energy balance is expressed as:

$$132 \quad R_n = H + \lambda E + G = (1 + \text{Bo})\lambda E + G. \quad (10)$$

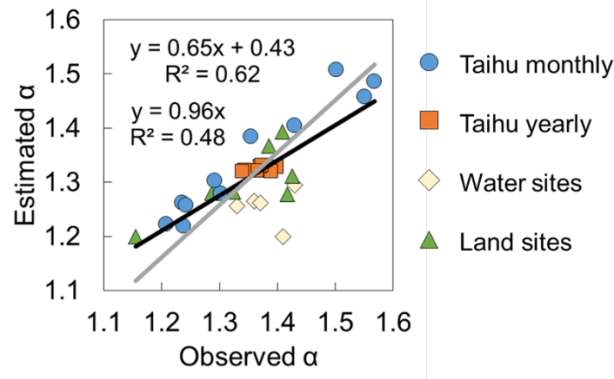
133 Combining Equations (2) and (10), α can be calculated as:

$$134 \quad \alpha = \frac{1}{1 + \text{Bo}} \frac{\varepsilon_a + 1}{\varepsilon_a}. \quad (11)$$

135 With Equation (9) and (11), we can derive the formula for α :

$$136 \quad \alpha = \begin{cases} 1, \text{equilibrium} \\ 1 + \frac{(\varepsilon_a \Lambda + 1)\chi}{\varepsilon_a [\varepsilon_a + 1 + (1 - \Lambda)\chi]}, \text{non-equilibrium} \end{cases} \quad (12)$$

137 Equation (12) is one of the main results in this study, and it can estimate α well compared
 138 to a large number of observations (Figure 2, please see the description of observed data
 139 in Section 3).



140

141 Figure 2. Comparison between observed and Equation (12) calculated α . The black line
 142 is the linear fitting with intercept and the gray line is the linear fitting through origin. The
 143 observed α is inversed by the PT model.

144 2.3 The sensitivity of α to air temperature and humidity

145 According to the above derivations, we can know that α is not a constant and it changes
 146 with T and Q. The sensitivity of α to T and Q, $d\alpha/dT$ and $d\alpha/dQ$, determines the variation
 147 of α if the initial α value is given. In this section, we derive explicit equations to estimate
 148 $d\alpha/dT$ and $d\alpha/dQ$.

149 Firstly, we decompose α changes in that of T and Q with partial differential equations
 150 based on Equation (11):

$$151 \quad \frac{\partial \alpha}{\partial T} = -\frac{1}{(1 + \text{Bo}_{\text{ABL}})^2} \frac{\varepsilon_a + 1}{\varepsilon_a} \frac{\partial \text{Bo}_{\text{ABL}}}{\partial T} - \frac{1}{\varepsilon_a^2} \frac{1}{1 + \text{Bo}_{\text{ABL}}} \frac{\partial \varepsilon_a}{\partial T}, \quad (13)$$

$$152 \quad \frac{\partial \alpha}{\partial Q} = -\frac{1}{(1 + \text{Bo}_{\text{ABL}})^2} \frac{\varepsilon_a + 1}{\varepsilon_a} \frac{\partial \text{Bo}_{\text{ABL}}}{\partial Q}, \quad (14)$$

153 where partial differential terms of $\frac{\partial \text{Bo}_{\text{ABL}}}{\partial T}$ and $\frac{\partial \text{Bo}_{\text{ABL}}}{\partial Q}$ can be estimated based on

154 Equation (9) as:

$$155 \quad \frac{\partial \text{Bo}_{\text{ABL}}}{\partial T} = -\frac{1 - \Lambda \chi}{(\varepsilon_a + \chi)^2} \frac{\partial \varepsilon_a}{\partial T}, \quad (15)$$

$$156 \quad \frac{\partial \text{Bo}_{\text{ABL}}}{\partial Q} = -\frac{\Lambda \varepsilon_a + 1}{(\varepsilon_a + \chi)^2} \frac{\partial \chi}{\partial Q}. \quad (16)$$

157 where terms of $\frac{\partial \varepsilon_a}{\partial T}$ and $\frac{\partial \chi}{\partial Q}$ can be approximated as:

$$158 \quad \frac{\partial \varepsilon_a}{\partial T} = \frac{1}{\gamma} \frac{\partial \Delta}{\partial T}, \quad (17)$$

$$159 \quad \frac{\partial \chi}{\partial Q} = \frac{\lambda}{c_p \gamma_v h}, \quad (18)$$

160 where Δ can be calculated as:

$$161 \quad \Delta = \frac{4098 e_s}{(T + 237.3)^2}. \quad (19)$$

162 Combining Equation (13)-(18), we can obtain:

$$163 \quad \frac{\partial \alpha}{\partial T} = \frac{1}{\gamma} \left[\frac{1}{(1 + \text{Bo}_{\text{ABL}})^2} \frac{1 - \Lambda \chi}{(\varepsilon_a + \chi)^2} \frac{\varepsilon_a + 1}{\varepsilon_a} - \frac{1}{\varepsilon_a^2} \frac{1}{1 + \text{Bo}_{\text{ABL}}} \right] \frac{\partial \Delta}{\partial T} \quad (20)$$

$$164 \quad \frac{\partial \alpha}{\partial Q} = \frac{1}{(1 + \text{Bo}_{\text{ABL}})^2} \frac{\Lambda \varepsilon_a + 1}{(\varepsilon_a + \chi)^2} \frac{\varepsilon_a + 1}{\varepsilon_a} \frac{\lambda}{c_p \gamma_v h} \quad (21)$$

165 We can rewrite the Equation (20) as follows:

$$166 \quad \frac{\partial \alpha}{\partial T} = -\frac{1}{\gamma} \frac{\chi \left[\varepsilon_a (\Lambda \varepsilon_a + 2) + \chi (1 - \Lambda) + 1 \right]}{(1 + \text{Bo}_{\text{ABL}})^2 (\varepsilon_a + \chi)^2 \varepsilon_a^2} \frac{\partial \Delta}{\partial T}, \quad (22)$$

167 The total differentiation of α is:

$$168 \quad d\alpha = \frac{\partial \alpha}{\partial T} dT + \frac{\partial \alpha}{\partial Q} dQ, \quad (23)$$

169 thus $\frac{d\alpha}{dT}$ and $\frac{d\alpha}{dQ}$ can be written as:

$$170 \quad \frac{d\alpha}{dT} = \frac{\partial \alpha}{\partial T} + \frac{\partial \alpha}{\partial Q} \frac{dQ}{dT}, \quad (24)$$

$$171 \quad \frac{d\alpha}{dQ} = \frac{\partial \alpha}{\partial Q} + \frac{\partial \alpha}{\partial T} \frac{dT}{dQ}. \quad (25)$$

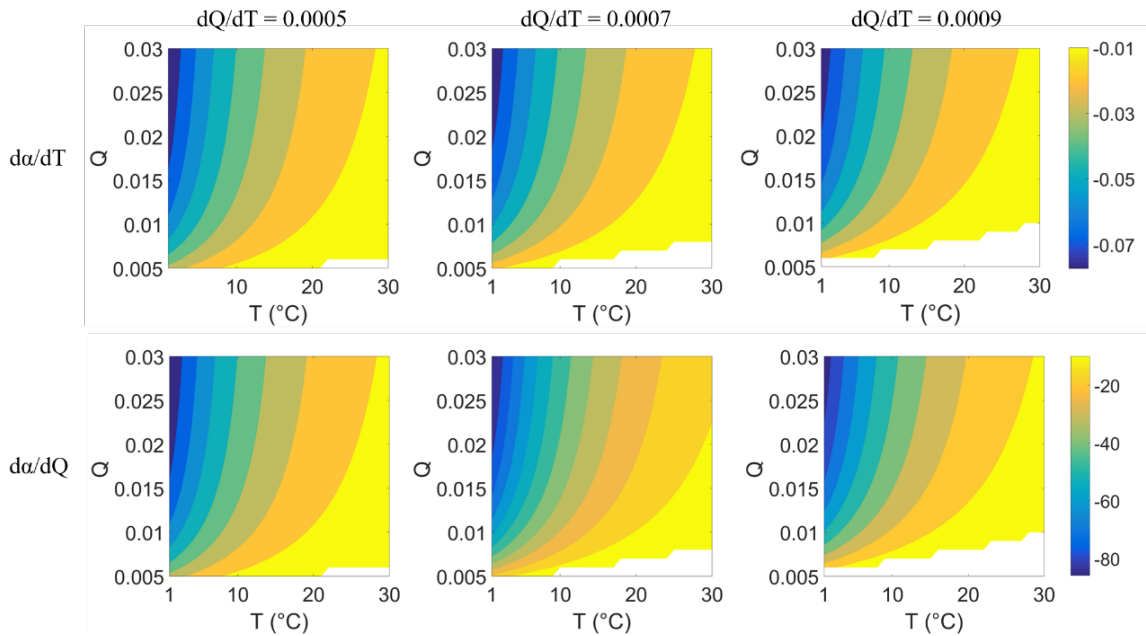
172 With the above equations, we can get theoretical relationships among α , T, and Q. This
 173 derivation can provide a simple and physically clear estimation for α changes. We also
 174 obtained $d\alpha/dT$ and $d\alpha/dQ$ values by fitting measured data using the linear regression
 175 model.

176 For practical use, we simplified the Equation (20) and (21) as:

$$177 \quad \frac{\partial \alpha}{\partial T} = -\frac{1}{\gamma} \frac{\chi}{\varepsilon_a + \chi} \frac{1}{\varepsilon_a^2} \frac{\partial \Delta}{\partial T} \quad (26)$$

$$178 \quad \frac{\partial \alpha}{\partial Q} = \frac{\varepsilon_a + 1}{\varepsilon_a (\varepsilon_a + \chi + 1)^2} \frac{\chi}{Q} \quad (27)$$

179 We further gave a numerical plot to show how α changes with T and Q (Figure 3). We
 180 plot this figure by setting a dQ/dT gradient from 0.0005, 0.0007, and 0.0009/K to ensure
 181 cover most of the cases over water surfaces. Figure 3 can be used as the lookup graphs to
 182 directly find $d\alpha/dT$ and $d\alpha/dQ$ values. For example, for a water surface with dQ/dT
 183 about 0.0007 /K, the values of $d\alpha/dT$ and $d\alpha/dQ$ can be found in the second column
 184 of Figure 3.



185

186 Figure 3. Values of $d\alpha/dT$ and $d\alpha/dQ$ under different T and Q . The first and second
 187 rows are $d\alpha/dT$ and $d\alpha/dQ$, respectively. The first to third columns are under different
 188 correlations between Q and T (dQ/dT) as 0.0005, 0.0007, and 0.0009/K, respectively.
 189 The blank space in each subpanel refers to values of $d\alpha/dT$ and $d\alpha/dQ$ are negative,
 190 indicating situations that rarely happen in the real world (i.e., with a very high temperature,
 191 the specific humidity is hardly deficient over wet surfaces).

192 3. Cases and applications

193 3.1 Data

194 We select data from eddy covariance measurements on several water surfaces [*Han and*
 195 *Guo, 2023*]: (i) Lake Taihu, located in the Yangtze River Delta, China, with an area of

196 $\sim 2,400 \text{ km}^2$, an average depth of 1.9 m [Lee *et al.*, 2014]. There are five sites over the
 197 Taihu surface, and the poor-quality data marked with quality flags are removed. (ii) Lake
 198 Poyang, located in the Yangtze Plain, China, with an area of $\sim 3,000 \text{ km}^2$ and an average
 199 depth of 8.4 m [X Zhao and Liu, 2018]. (iii) Erhai, located in the Yun-Gui Plateau of
 200 China, with an area of $\sim 250 \text{ km}^2$ and an average depth of 10 m [Du *et al.*, 2018]. (iv)
 201 Guandu Ponds, located in Anhui Province, China, with an area of $\sim 0.05 \text{ km}^2$ and an
 202 average depth of 0.8 m [J Zhao *et al.*, 2019]; (v) Lake Suwa, located in Nagano, Japan,
 203 with an area of $\sim 13 \text{ km}^2$ and an average depth of 4 m [Taoka *et al.*, 2020]. Months with
 204 negative values of sensible heat fluxes have not remained. The latitude, longitude, and
 205 available data period of five lakes/ponds are listed in Table 1. For α changes in time, we
 206 use data from Lake Taihu for investigation due to its sufficient data length. For α changes
 207 in space, we calculate the average temperature, specific humidity, and α of each lake for
 208 comparison.

209 Table 1. Location and date period of each water body.

Site	Lat ($^{\circ}$)	Lon ($^{\circ}$)	Size (km^2)	Periods ^a	Sample size (number of months)
Taihu	31.23	120.11	3000	2012.01 - 2018.12	341 ^b
Poyang	29.08	116.40	2400	2013.08 - 2017.09	41
Erhai	25.77	100.17	250	2012.01 - 2018.12	24 ^c
Guandu	31.97	118.25	0.05	2017.06 - 2019.12	31
Suwa	36.05	138.11	13	2016.01 - 2018.12	36

210 Note: a. Periods refer to the date of the first measurement to the date of the last one,
 211 including months for which no data are available. b. There are five eddy covariance sites
 212 over lake Taihu. c. Only climatology monthly data from two periods of 2012-2015 and
 213 2015-2018 are available.

214 Observations from global flux sites (FluxNet2015 database) are also selected. We first
 215 examine days without water stress based on the following steps [Maes *et al.*, 2019]. At
 216 each site, the evaporative fraction EF (i.e., latent heat flux over the sum of latent and
 217 sensible fluxes) is first calculated, and the days with EF exceeding the 95th percentile EF
 218 and with EF larger than 0.8 remain. Secondly, the days with soil moisture lower than 50%
 219 of the maximum soil moisture (taken as the 98th percentile of the soil moisture series) are
 220 removed. Days having rainfall and negative values of latent and sensible heat fluxes are
 221 also not included. As a result, a total of ~ 700 non-water-stressed site-days pass the
 222 criterion. Data is divided into seven vegetation types including croplands (CRO),
 223 wetlands (WET), evergreen needleleaf and mixed forests (DNF_MF), evergreen
 224 broadleaf and deciduous broadleaf forests (EBF_DBF), grasslands (GRA), close
 225 shrublands (CSH), and woody savanna (WSA), to analyze α changes in space. It should
 226 be noted that we do not average the daily data to a monthly scale due to variations in data

227 sizes across different months for a specific site. Instead, we organize the selected daily
 228 data by vegetation types, as the primary objective of utilizing land fluxes data is to assess
 229 the derived relationship spatially rather than temporally.

230 We also collect ocean surface data from 11 CMIP6 models (under scenario SSP585, Table
 231 2) from 2021-2100 to see the temporal changes in α . The calculation is limited to the
 232 latitudinal range 60°S to 60°N, and takes all ocean surface grids as a whole [Roderick *et*
 233 *al.*, 2014]. We average the monthly data to the yearly scale and calculate α every ten years
 234 from 2021 to 2100 (i.e., 2021-2030, 2031-2040, etc.).

235 Table 2. CMIP6 models used in this study.

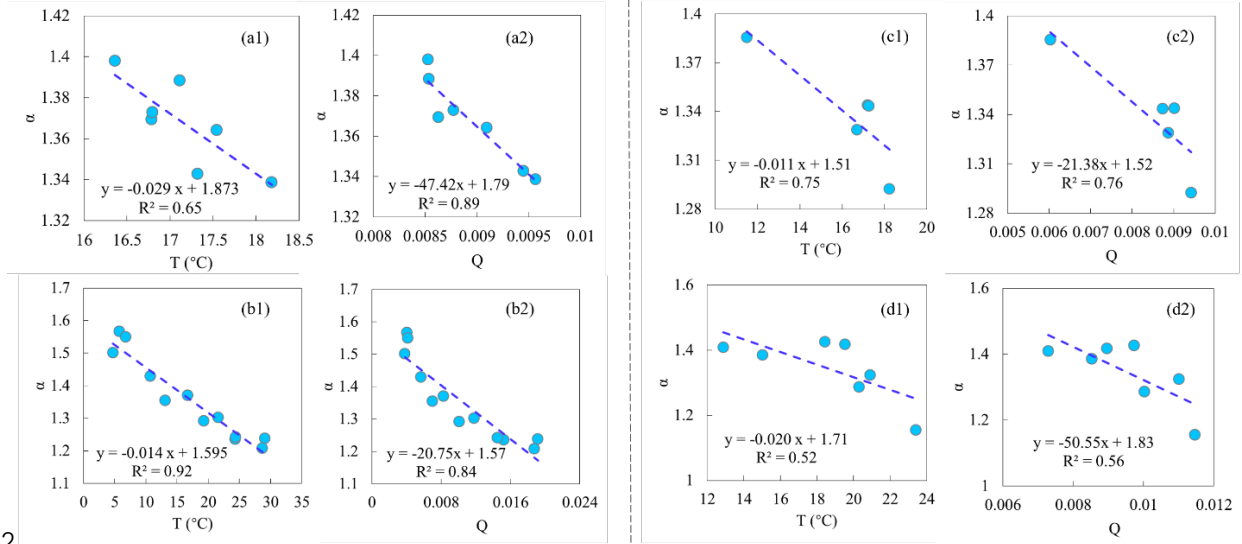
Model	Nation	Institute
ACCESS-ESM1-5	Australia	CSIRO
CanESM5	Canada	CCCma
CESM2-WACCM	USA	NCAR
CMCC-CM2-SR5	Italy	CMCC
CMCC-ESM2	Italy	CMCC
FGOALS-g3	China	CAS
FIO-ESM-2-0	China	CAS
MPI-ESM1-2-HR	Germany	MPI-M
MPI-ESM1-2-LR	Germany	MPI-M
NorESM2-LM	Norway	NCC
NorESM2-MM	Norway	NCC

236 Note: CSIRO: Commonwealth Scientific and Industrial Research Organization;
 237 CCCma: Canadian Centre for Climate Modelling and Analysis; NCAR: National Center
 238 for Atmospheric Research; CMCC: Euro-Mediterranean Center on Climate Change;
 239 CAS: Chinese Academy of Sciences; MPI-M: Max Planck Institute for Meteorology;
 240 NCC: Norwegian Climate Centre.

241 3.2 Results

242 (1) Temporal and spatial changes in α

243 We used yearly and climatology monthly (from Jan to Dec) data from Lake Taihu to
 244 investigate the temporal variation in α . α is firstly inversed by the PT model and
 245 measurements, and then we found significant negative relationships of α with both T and
 246 Q (Figure 4). On the yearly scale, the regressed values of $d\alpha/dT$ and $d\alpha/dQ$ are -
 247 0.029/°C and -47.42, and the values on the seasonal scale are -0.014/°C and -20.75,
 248 respectively. $d\alpha/dT$ on the seasonal scale is higher than that on the yearly scale because
 249 the variation range of α on the seasonal scale is more extensive. Theoretical derived $d\alpha/dT$
 250 and $d\alpha/dQ$ roughly match with the regressed values (Table 3). We also analyzed on the
 251 ten-day scale and obtained robust results (Figure S1 and Table S1).



252

253 Figure 4. Temporal and spatial relationships of α and temperature (T) and specific
 254 humidity (Q). (a-b) Temporal relationships based on lake Taihu data: (a) yearly data, and
 255 (b) climatology monthly data. (c-d) Spatial relationships: (c) data from five water surface
 256 sites, and (d) land surface data from FluxNet2015, each circle representing one vegetation
 257 type. The linear regression line and correlation coefficient (R^2) are shown in each
 258 subpanel.

259

260 Table 3 Sensitivity of α to temperature (T) and specific humidity (Q) by regression and
 261 theoretical derivation.

		$d\alpha/dT$ ($^{\circ}C$)		$d\alpha/dQ$	
		regression	derivation	regression	derivation
Temporal	yearly	-0.029	-0.023	-47.42	-37.95
	seasonally	-0.014	-0.011	-20.75	-18.38
Spatial	water sites	-0.011	-0.012	-21.38	-24.30
	land sites	-0.020	-0.016	-50.55	-40.47

262

263 Spatial relationships of α with T and Q are similar to that in time, i.e., higher T and Q
 264 generally correspond to lower α , supported by measurements over both water and land
 265 surfaces (Figure 4). For the water surfaces, the values of $d\alpha/dT$ and $d\alpha/dQ$ are -
 266 $0.011/^{\circ}C$ and -21.38 , and the values for land surfaces are $-0.020/^{\circ}C$ and -50.55 . The
 267 derived $d\alpha/dT$ and $d\alpha/dQ$ reasonably match well with the regressed values (Table 3).
 268 The correlations (represented by R^2 in Figure 4) between α and T, α and Q of water
 269 surfaces are higher than those over the land surfaces. This indicates that changes in α are
 270 more associated with T and Q over water surfaces, which may be because T and Q
 271 dominate the water surface evaporation process, while some other factors, like vegetation
 272 and wind speed, also play specific roles over land surfaces.

273 Based on Equation (20) to (22), $\partial\alpha/\partial T$ is always a negative value, and $\partial\alpha/\partial Q$ is

274 always positive. The regressed and derived $d\alpha/dT$ and $d\alpha/dQ$ are both negative.
 275 Combined with Equations (24), (25) and the positive relationship between T and Q, the
 276 $\partial\alpha/\partial T$ plays a more critical role in determining (the signs of) $d\alpha/dT$ and $d\alpha/dQ$, that
 277 is, $|\partial\alpha/\partial T| > \partial\alpha/\partial Q \cdot dQ/dT$ and $|\partial\alpha/\partial T \cdot dT/dQ| > \partial\alpha/\partial Q$. Specifically, based on the data
 278 from lake Taihu (for detecting α changes in time) and data from different water surface
 279 sites and land surface sites (for detecting α changes in space), we found the contribution
 280 of $\partial\alpha/\partial T \cdot dT$ to $d\alpha$ is $\sim 70\%$, much more significant than that of $\partial\alpha/\partial Q \cdot dQ$ of $\sim 30\%$
 281 (Table 4). Therefore, according to the evaporation process over the wet surface (Section
 282 2.1) and the above analyses, we can conclude that α is fundamentally controlled by T and
 283 modulated by Q.

284 Table 4. Contributions of changes in temperature (T) and specific humidity (Q) to
 285 changes in α .

		$d\alpha$	contribution of $\frac{\partial\alpha}{\partial T}dT$	contribution of $\frac{\partial\alpha}{\partial Q}dQ$
Temporal	yearly	-0.035	78%	22%
	seasonally	-0.256	67%	33%
Spatial	water sites	-0.081	68%	32%
	land sites	-0.167	77%	23%
Average		----	72.5%	27.5%

286 Note: Since $d\alpha = \frac{\partial\alpha}{\partial T}dT + \frac{\partial\alpha}{\partial Q}dQ$, the contribution of $\frac{\partial\alpha}{\partial T}dT$ is calculated as

287 $\left| \frac{\partial\alpha}{\partial T}dT \right| / \left| \frac{\partial\alpha}{\partial T}dT + \frac{\partial\alpha}{\partial Q}dQ \right|$, and is the contribution of $\frac{\partial\alpha}{\partial Q}dQ$ calculated as

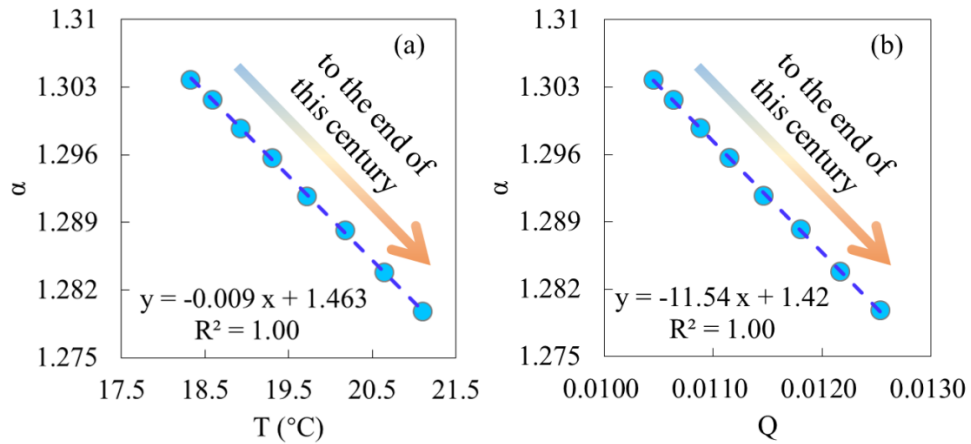
288 $\left| \frac{\partial\alpha}{\partial Q}dQ \right| / \left| \frac{\partial\alpha}{\partial T}dT + \frac{\partial\alpha}{\partial Q}dQ \right|$. $d\alpha$ refers to the estimated variation of α from lowest to highest

289 T (also from lowest to highest Q since T and Q are positively correlated).

290 Derived $d\alpha/dT$ and $d\alpha/dQ$ have more or less errors compared to the regressed values.
 291 Several reasons can explain this: (i) errors in measurements of eddy covariance systems;
 292 (ii) the additional factors other than T and Q, like wind speed, can also influence α ; (iii)
 293 the relationship of α and T (also α and Q) cannot be well represented by the linear
 294 regression model. Besides, the water surface size effects on evaporation and α , reported
 295 by *Han and Guo* [2023], are not well considered in the presented derivation. Nevertheless,
 296 the derived expression can fairly match the observations of water bodies with various
 297 sizes (Table 3).

298 **(2) Potential applications for global projections**

299 Based on CMIP6 ocean surface data, we also detected significant negative relationships
 300 of α with T and Q (Figure 5). $d\alpha/dT$ and $d\alpha/dQ$ obtained by the linear regression are
 301 $-0.009/^\circ\text{C}$ and -11.54 , respectively. The derived $d\alpha/dT$ and $d\alpha/dQ$ are close to the
 302 regressed value as $-0.009/^\circ\text{C}$ and -10.74 . We further compared the changes in T, Q, and
 303 heat fluxes between the first and the last ten years in 2021-2100 (Table 5). To the end of
 304 this century, CMIP6 models predict that ocean average available energy (R_n-G) and latent
 305 heat flux (also evaporation) will increase by $\sim 3.1 \text{ W/m}^2$ and $\sim 6.0 \text{ W/m}^2$, respectively.
 306 Using the PT model with the fixed α (1.26), predicted evaporation shows an increase of
 307 $\sim 8.0 \text{ W/m}^2$, far higher than climate models' direct output (with a relative bias of $\sim 30\%$).
 308 Based on derived α , ocean evaporation shows a much smaller increase of $\sim 5.8 \text{ W/m}^2$, with
 309 less than 5% relative bias compared to CMIP6 values (Figure 6). This indicates that
 310 changes in α should be well considered for the long-term projections. So here we suggest
 311 introducing the negative relationship between α and T, proposed in this study, into the
 312 original PT model to correct for the overestimated sensitivity of evaporation to
 313 temperature [Z Liu et al., 2022], which could also improve the reliability of global long-
 314 term drought predictions [Greve et al., 2019].



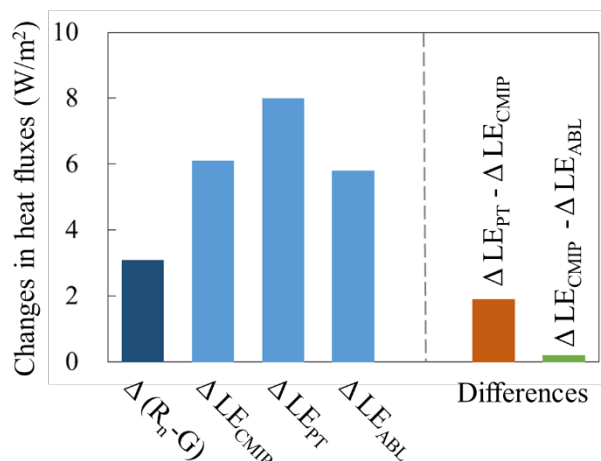
315
 316 Figure 5. Temporal relationship of (a) α and temperature (T), and (b) α and specific
 317 humidity (Q) over global ocean surfaces. Each dot denotes the data in each 10-year
 318 window (2021-2030, 2031-2041, ..., 2091-2100), from left to right is from 2021-2030 to
 319 2091-2100.

320
 321 Table 5. Ocean surface temperature, specific humidity, and heat fluxes at the first ten
 322 years (2021-2030) and the end of the 21st century (2091-2100). T, Q, R_n-G , and LE are
 323 direct outputs of climate models. α -CMIP refers to α inverted by the PT model with CMIP
 324 data. LE_{PT} is calculated by the PT model with fixed α at 1.26. α -ABL refers to α estimated
 325 by the ABL model. LE_{ABL} is calculated by the PT model with α -ABL.

Period	T	Q	R_n-G	LE	α -CMIP	LE_{PT}	α -ABL	LE_{ABL}
	($^\circ\text{C}$)	(-)	(W/m^2)	(W/m^2)		(W/m^2)		(W/m^2)

2021-2030	18.1	0.010	122.9	106.8	1.304	103.2	1.316	107.7
2091-2100	21.1	0.013	126.0	112.9	1.279	111.2	1.287	113.5
Δ	3.0	0.003	3.1	6.1	-0.025	8.0	-0.029	5.8

326



327

328 Figure 6. Stylized diagram showing the average changes in heat fluxes over global
 329 ocean surfaces.

330 4. Discussions and Conclusions

331 In this study, we employed an open boundary layer model with a governing potential VPD
 332 budget [Raupach, 2000; 2001], originally integrated by Z Liu and Yang [2021], to
 333 formulate an expression for the Priestley-Taylor coefficient, α . Notably, the governing
 334 equation allows the derived expression has no calibrated parameters and can estimate a
 335 precise α value with normal observations, rendering it superior to other methods that also
 336 built with the boundary layer theory [J. P. Lhomme, 1997b; Chiel C. van Heerwaarden et
 337 al., 2009]. With the expression and a variety of measurements, we further demonstrated
 338 that temperature exerts a more significant influence on variations in α , as opposed to
 339 specific humidity. We suggest that for studies focusing on evaporation and/or drought
 340 projections, it is crucial to thoroughly characterize the negative correlation between α and
 341 temperature, a relationship easily determined using the derived expression.

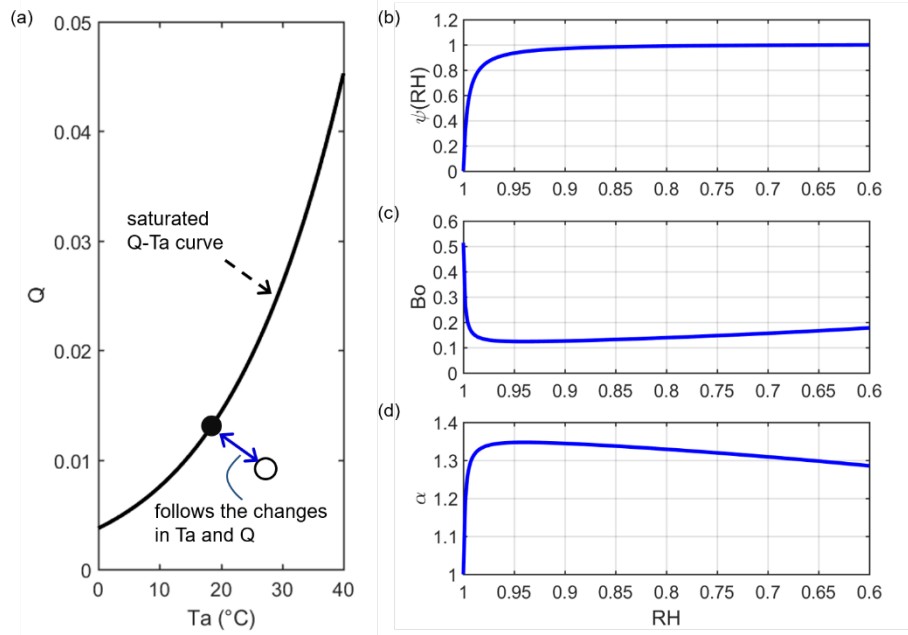
342 It should be noted that except for the PT model, the PM-based model can be also used to
 343 estimate wet surface evaporation [Penman, 1948; Shuttleworth, 1993]. While PM-based
 344 equations encapsulate all processes that possibly affect evaporation, the PT model, taking
 345 evaporation as a simple function of radiation and temperature, takes more account of the
 346 feedback/balance between the surface and near atmosphere (Figure 1). Besides, it has
 347 been noted that the PM-based models may fail at certain limits, and cannot capture the
 348 sensitivity of evaporation to temperature changes (Liu et al., 2022; McColl, 2020). So in
 349 this case, also with the fact that the PT model is currently one of the most popular

350 equations due to its low input requirements, revisiting this classic model can greatly
 351 promote its adaption under the changing climate.

352 In Section 2.1, it was suggested that $\Delta_D = 0$ for the saturated air while $\Delta_D \approx Q$ for the
 353 non-saturated air. In theory, it is expected that the transition track between saturated and
 354 non-saturated states should be continuous and smooth. That is, the changes in the value
 355 of Δ_D between the saturated (0) and non-saturated (Q) states should follow the
 356 variations in air energy and moisture (Figure 7). Since the relative humidity (RH) includes
 357 both information on air temperature and humidity, here we introduce a possible track of
 358 Δ_D depending on RH as: $\Delta_D = \psi(\text{RH}) \cdot Q$. As we expect, the value of Δ_D approaches 0
 359 when the air is very moist (i.e., very close to the saturated state and RH close to 1), so ψ
 360 should be a nonlinear and monotone convex function of RH. We give a possible
 361 expression of $\psi(\text{RH})$ as:

$$362 \quad \psi(\text{RH}) = 1 - \frac{1}{1 + m \times \left(\frac{\text{RH}_{\max} - \text{RH}}{\text{RH} - \text{RH}_{\min}} \right)^n} \quad (28)$$

363 where RH_{\max} is 1, and RH_{\min} is 0.6 [McColl and Tang, 2023] over the water surfaces. m
 364 and n are shape parameters. To make $\psi(\text{RH})$ simple, we fixed n at 1, and let m be 100.
 365 The relationship between $\psi(\text{RH})$ and RH can be viewed in Figure 7 (b). For a specific
 366 case that T at 18 °C, we show the changes in Bo and α with RH in Figure 7 (c)-(d).
 367 Although there is a dramatic shift in Bo or α , it appears when RH is at 0.95-1, which is
 368 outside the vast majority of actual cases (RH is generally smaller than 0.9 on a monthly
 369 or longer scale). After the shift point, with RH decreases, $\psi(\text{RH})$, Bo , and α remain
 370 roughly stable. It is worth noting that Equation (28) (with specific parameters) is one
 371 possible case that connects the transition between saturated and non-saturated air states,
 372 a fine determination may be affected by local conditions, but Δ_D value around Q is
 373 expected for most of the cases.



374

375 Figure 7. (a) Transition between saturated and non-saturated air states. The filled circle
 376 represents one case in which the air is saturated (saturated state) and the open circle
 377 represents one case in which air is not saturated (non-saturated state). (b) Relationship
 378 between $\psi(RH)$ and RH with Equation (28). (c)-(d) Changes in Bo and α as the
 379 function of RH when air temperature is fixed at 18 °C.

380 We recommend utilizing the derived model under warm conditions, for example, when
 381 the air temperature exceeds zero, to account for the prerequisite of a well-mixed boundary
 382 layer. In extremely cold regions or seasons, the water surface temperature can be lower
 383 than the air temperature, resulting in a downward sensible heat flux [*de Bruin, 1982*].
 384 Under such circumstances, the boundary layers exhibit relative stability and may not
 385 reach a well-mixed state. Additionally, we advise adopting a temporal scale ranging from
 386 weekly to monthly when applying the derived model. This is because the potential VPD
 387 budget (the governing equation) may not be rapidly achieved, such as on a diurnal or daily
 388 basis. Furthermore, over a longer term, the sensible heat flux typically manifests as
 389 upward in the majority of scenarios than on a fine temporal scale.

390 The derived formula for α has important practical meanings. For example, it would be
 391 useful for estimating water surface evaporation and actual evapotranspiration based on
 392 the PT model [*Maes et al., 2019; Miralles et al., 2011*]. It can also help to constrain the
 393 relationships among α , T , and Q in the complementary relationship, whose performance
 394 previously depended on the inversed α [*X Liu et al., 2016*]. Besides, considering the
 395 impacts of changing climate on α can significantly improve the performance of the
 396 hydrologic model in runoff simulations and predictions [*Pimentel et al., 2023*].

397 **Author Contributions**

398 Conceptualization: Ziwei Liu, Hanbo Yang. Data curation: Ziwei Liu. Formal analysis:
399 Ziwei Liu. Funding acquisition: Hanbo Yang. Methodology: Ziwei Liu, Hanbo Yang.
400 Software: Ziwei Liu. Supervision: Hanbo Yang. Writing – original draft: Ziwei Liu.
401 Writing – review & editing: Changming Li, Taihua Wang, Hanbo Yang.

402 **Data availability**

403 Data of Lake Taihu can be obtained from Harvard Dataverse,
404 <https://doi.org/10.7910/DVN/HEWCWM>. The data of Poyang Lake can be obtained
405 from *X Zhao and Liu* [2018] and *Gan and Liu* [2020]. The data of Erhai can be obtained
406 from *Du et al.* [2018]. The data of Guandu can be obtained from *J Zhao et al.* [2019].
407 The data of Suwa lake can be obtained from the AsiaFlux
408 (http://asiaflux.net/index.php?page_id=1355). FluxNet 2015 data are available at
409 <https://fluxnet.fluxdata.org/data/download-data/>. CMIP6 data can be obtained from
410 Earth System Grid Federation (<https://esgf-node.llnl.gov>).

411 **Acknowledgments**

412 This study is financially supported by the National Natural Science Foundation of China
413 (grant nos. 51979140, 42041004).

414 **Competing interests**

415 There are no competing interests.

416 **References:**

- 417 Andreas, E. L., and B. A. Cash (1996), A new formulation for the Bowen ratio over saturated surfaces,
418 *Journal of Applied Meteorology*, 35(8), 1279-1289, doi:10.1175/1520-
419 0450(1996)035<1279:anfftb>2.0.co;2.
- 420 Assouline, S., D. Li, S. Tyler, J. Tanny, S. Cohen, E. Bou-Zeid, M. Parlange, and G. G. Katul (2016), On
421 the variability of the Priestley-Taylor coefficient over water bodies, *Water Resources Research*, 52(1), 150-
422 163, doi:10.1002/2015wr017504.
- 423 Bowen, I. S. (1926), The ratio of heat losses by conduction and by evaporation from any water surface,
424 *Physical Review*, 27(6), 779-787, doi:10.1103/PhysRev.27.779.
- 425 Brutsaert, W., and H. J. W. r. r. Stricker (1979), An advection-aridity approach to estimate actual regional
426 evapotranspiration, 15(2), 443-450.
- 427 Crago, R. D., J. Szilagyi, and R. J. Qualls (2023), What is the Priestley–Taylor wet-surface evaporation
428 parameter? Testing four hypotheses, *Hydrol. Earth Syst. Sci.*, 27(17), 3205-3220, doi:10.5194/hess-27-
429 3205-2023.
- 430 de Bruin, H. A. R. (1982), Temperature and energy balance of a water reservoir determined from standard
431 weather data of a land station, *Journal of Hydrology*, 59(3), 261-274, doi:[https://doi.org/10.1016/0022-
432 1694\(82\)90091-9](https://doi.org/10.1016/0022-1694(82)90091-9).
- 433 Debruin, H. A. R., and J. Q. Keijman (1979), PRIESTLEY-TAYLOR EVAPORATION MODEL APPLIED
434 TO A LARGE, SHALLOW LAKE IN THE NETHERLANDS, *Journal of Applied Meteorology*, 18(7),
435 898-903, doi:10.1175/1520-0450(1979)018<0898:Tptema>2.0.Co;2.
- 436 Du, Q., H. Z. Liu, Y. Liu, L. Wang, L. J. Xu, J. H. Sun, and A. L. Xu (2018), Factors controlling evaporation
437 and the CO₂ flux over an open water lake in southwest of China on multiple temporal scales, *International
438 Journal of Climatology*, 38(13), 4723-4739, doi:10.1002/joc.5692.
- 439 Eichinger, W. E., M. B. Parlange, and H. Stricker (1996), On the concept of equilibrium evaporation and
440 the value of the Priestley-Taylor coefficient, *Water Resources Research*, 32(1), 161-164.
- 441 Gan, G., and Y. Liu (2020), Heat Storage Effect on Evaporation Estimates of China's Largest Freshwater
442 Lake, 125(19), e2019JD032334, doi:<https://doi.org/10.1029/2019JD032334>.
- 443 Greve, P., M. L. Roderick, A. M. Ukkola, and Y. Wada (2019), The aridity Index under global warming,
444 *Environmental Research Letters*, 14(12), doi:10.1088/1748-9326/ab5046.
- 445 Guo, X., H. Liu, and K. J. B.-L. M. Yang (2015), On the application of the Priestley–Taylor relation on sub-
446 daily time scales, 156, 489-499.
- 447 Han, S., and F. Guo (2023), Evaporation From Six Water Bodies of Various Sizes in East Asia: An Analysis
448 on Size Dependency, *Water Resources Research*, 59(6), doi:10.1029/2022wr032650.
- 449 Hicks, B. B., and G. D. Hess (1977), On the Bowen Ratio and Surface Temperature at Sea, *Journal of
450 Physical Oceanography*, 7(1), 141-145, doi:10.1175/1520-0485(1977)007<0141:otbras>2.0.co;2.
- 451 Jury, W., and C. J. A. J. Tanner (1975), Advection Modification of the Priestley and Taylor
452 Evapotranspiration Formula 1, 67(6), 840-842.
- 453 Lee, X., et al. (2014), THE TAIHU EDDY FLUX NETWORK An Observational Program on Energy, Water,
454 and Greenhouse Gas Fluxes of a Large Freshwater Lake, *Bulletin of the American Meteorological Society*,
455 95(10), 1583-1594, doi:10.1175/bams-d-13-00136.1.
- 456 Lhomme, J. P. (1997a), An examination of the Priestley-Taylor equation using a convective boundary layer
457 model, *Water Resources Research*, 33(11), 2571-2578.

- 458 Lhomme, J. P. (1997b), A THEORETICAL BASIS FOR THE PRIESTLEY-TAYLOR COEFFICIENT,
459 *Boundary-Layer Meteorology*, 82(2), 179-191, doi:10.1023/A:1000281114105.
- 460 Liu, X., C. Liu, and W. Brutsaert (2016), Regional evaporation estimates in the eastern monsoon region of
461 China: Assessment of a nonlinear formulation of the complementary principle, 52(12), 9511-9521,
462 doi:<https://doi.org/10.1002/2016WR019340>.
- 463 Liu, Z., J. Han, and H. Yang (2022), Assessing the ability of potential evaporation models to capture the
464 sensitivity to temperature, *Agricultural and Forest Meteorology*, 317, 108886.
- 465 Liu, Z., and H. Yang (2021), Estimation of Water Surface Energy Partitioning With a Conceptual
466 Atmospheric Boundary Layer Model, *Geophysical Research Letters*, 48(9), e2021GL092643,
467 doi:<https://doi.org/10.1029/2021GL092643>.
- 468 Maes, W. H., P. Gentine, N. E. C. Verhoest, and D. G. Miralles (2019), Potential evaporation at eddy-
469 covariance sites across the globe, *Hydrology and Earth System Sciences*, 23(2), 925-948, doi:10.5194/hess-
470 23-925-2019.
- 471 McColl, K. A., and L. I. Tang (2023), An analytic theory of near-surface relative humidity over land,
472 *Journal of Climate*, doi:<https://doi.org/10.1175/JCLI-D-23-0342.1>.
- 473 McNaughton, K., and T. Spriggs (1986), A MIXED-LAYER MODEL FOR REGIONAL EVAPORATION,
474 *Boundary-Layer Meteorology*, 34(3), 243-262, doi:10.1007/bf00122381.
- 475 Miralles, D. G., T. Holmes, R. De Jeu, J. Gash, A. Meesters, A. J. H. Dolman, and E. S. Sciences (2011),
476 Global land-surface evaporation estimated from satellite-based observations, 15(2), 453-469.
- 477 Penman, H. L. (1948), Natural evaporation from open water, bare soil and grass, *Proceedings of the Royal*
478 *Society of London Series a-Mathematical and Physical Sciences*, 193(1032), 120-145,
479 doi:10.1098/rspa.1948.0037.
- 480 Pimentel, R., B. Arheimer, L. Crochemore, J. C. M. Andersson, I. G. Pechlivanidis, and D. Gustafsson
481 (2023), Which Potential Evapotranspiration Formula to Use in Hydrological Modeling World-Wide?, 59(5),
482 e2022WR033447, doi:<https://doi.org/10.1029/2022WR033447>.
- 483 Priestley, C. H. B., and R. J. Taylor (1972), Assessment of surface heat-flux and evaporation using large-
484 scale parameters, *Monthly Weather Review*, 100(2), 81-92, doi:10.1175/1520-
485 0493(1972)100<0081:otaosh>2.3.co;2.
- 486 Raupach, M. R. (2000), Equilibrium evaporation and the convective boundary layer, *Boundary-Layer*
487 *Meteorology*, 96(1-2), 107-141, doi:10.1023/a:1002675729075.
- 488 Raupach, M. R. (2001), Combination theory and equilibrium evaporation, *Quarterly Journal of the Royal*
489 *Meteorological Society*, 127(574), 1149-1181, doi:10.1256/smsqj.57401.
- 490 Roderick, M. L., F. Sun, W. H. Lim, and G. D. Farquhar (2014), A general framework for understanding
491 the response of the water cycle to global warming over land and ocean, *Hydrology and Earth System*
492 *Sciences*, 18(5), 1575-1589, doi:10.5194/hess-18-1575-2014.
- 493 Shuttleworth, W. J. (1993), Evaporation In: Maidment, DR Handbook of hydrology, edited, McGraw-Hill
494 New York.
- 495 Slatyer, R. O., and I. C. McIlroy (1961), *Practical microclimatology: with special reference to the water*
496 *factor in soil-plant-atmosphere relationships*, Melbourne: Commonwealth Scientific and Industrial
497 Research Organisation.
- 498 Su, Q., and V. P. Singh (2023), Calibration-Free Priestley-Taylor Method for Reference Evapotranspiration
499 Estimation, 59(3), e2022WR033198, doi:<https://doi.org/10.1029/2022WR033198>.
- 500 Taoka, T., H. Iwata, R. Hirata, Y. Takahashi, Y. Miyabara, and M. Itoh (2020), Environmental Controls of
501 Diffusive and Ebullitive Methane Emissions at a Subdaily Time Scale in the Littoral Zone of a Midlatitude
502 Shallow Lake, *Journal of Geophysical Research-Biogeosciences*, 125(9), doi:10.1029/2020jg005753.

- 503 Thornthwaite, C. W., and B. Holzman (1939), Evaporation from land and water surfaces, *Monthly Weather*
504 *Review*, 67, 4-11, doi:10.1175/1520-0493(1939)67<4:tdoefl>2.0.co;2.
- 505 van Heerwaarden, C. C., J. V. G. de Arellano, A. F. Moene, and A. A. M. Holtslag (2009), Interactions
506 between dry-air entrainment, surface evaporation and convective boundary-layer development, *Quarterly*
507 *Journal of the Royal Meteorological Society*, 135(642), 1277-1291, doi:10.1002/qj.431.
- 508 Xiao, W., Z. Zhang, W. Wang, M. Zhang, Q. Liu, Y. Hu, W. Huang, S. Liu, and X. Lee (2020), Radiation
509 Controls the Interannual Variability of Evaporation of a Subtropical Lake, *Journal of Geophysical*
510 *Research-Atmospheres*, 125(8), doi:10.1029/2019jd031264.
- 511 Yang, Y., and M. L. Roderick (2019), Radiation, surface temperature and evaporation over wet surfaces,
512 *Quarterly Journal of the Royal Meteorological Society*, 145(720), 1118-1129, doi:10.1002/qj.3481.
- 513 Zhao, J., et al. (2019), An evaluation of the flux-gradient and the eddy covariance method to measure CH₄,
514 CO₂, and H₂O fluxes from small ponds, *Agricultural and Forest Meteorology*, 275, 255-264,
515 doi:10.1016/j.agrformet.2019.05.032.
- 516 Zhao, X., and Y. Liu (2018), Variability of Surface Heat Fluxes and Its Driving Forces at Different Time
517 Scales Over a Large Ephemeral Lake in China, *Journal of Geophysical Research-Atmospheres*, 123(10),
518 4939-4957, doi:10.1029/2017jd027437.

519